

## Article

# A Competitive O-Acetylserine Sulfhydrylase Inhibitor Modulates the Formation of Cysteine Synthase Complex

Marialaura Marchetti <sup>1,\*</sup>, Francesco Saverio De Angelis <sup>2</sup>, Giannamaria Annunziato <sup>3</sup>, Gabriele Costantino <sup>3</sup>, Marco Pieroni <sup>3</sup>, Luca Ronda <sup>1,4,5</sup>, Andrea Mozzarelli <sup>3,5</sup>, Barbara Campanini <sup>1,3</sup>, Salvatore Cannistraro <sup>2</sup>, Anna Rita Bizzarri <sup>2,\*</sup> and Stefano Bettati <sup>1,4,5</sup>

- <sup>1</sup> Biopharmanet-TEC Interdepartmental Center, University of Parma, 43124 Parma, Italy; luca.ronda@unipr.it (L.R.); barbara.campanini@unipr.it (B.C.); stefano.bettati@unipr.it (S.B.)
- <sup>2</sup> Department of Biological and Ecological Sciences, University of Tuscia, 01100 Viterbo, Italy; deangelis.francesco.saverio@gmail.com (F.S.D.A.); cannistr@unitus.it (S.C.)
- <sup>3</sup> Department of Food and Drug, University of Parma, 43124 Parma, Italy; giannamaria.annunziato@unipr.it (G.A.); gabriele.costantino@unipr.it (G.C.); marco.pieroni@unipr.it (M.P.); andrea.mozzarelli@unipr.it (A.M.)
- <sup>4</sup> Department of Medicine and Surgery, University of Parma, 43126 Parma, Italy
- <sup>5</sup> Institute of Biophysics, CNR, 56124 Pisa, Italy
- \* Correspondence: marialaura.marchetti@unipr.it (M.M.); bizzarri@unitus.it (A.R.B.); Tel.: +39-05-2190-6197 (M.M.); +39-07-6135-7031 (A.R.B.)



**Citation:** Marchetti, M.; De Angelis, F.S.; Annunziato, G.; Costantino, G.; Pieroni, M.; Ronda, L.; Mozzarelli, A.; Campanini, B.; Cannistraro, S.; Bizzarri, A.R.; et al. A Competitive O-Acetylserine Sulfhydrylase Inhibitor Modulates the Formation of Cysteine Synthase Complex. *Catalysts* **2021**, *11*, 700. <https://doi.org/10.3390/catal11060700>

Academic Editors: Francesco Zaccaria and Martin Lamac

Received: 26 April 2021

Accepted: 28 May 2021

Published: 31 May 2021

**Publisher's Note:** MDPI stays neutral with regard to jurisdictional claims in published maps and institutional affiliations.



**Copyright:** © 2021 by the authors. Licensee MDPI, Basel, Switzerland. This article is an open access article distributed under the terms and conditions of the Creative Commons Attribution (CC BY) license (<https://creativecommons.org/licenses/by/4.0/>).

**Abstract:** Cysteine is the main precursor of sulfur-containing biological molecules in bacteria and contributes to the control of the cell redox state. Hence, this amino acid plays an essential role in microbial survival and pathogenicity and the reductive sulfate assimilation pathway is considered a promising target for the development of new antibacterials. Serine acetyltransferase (SAT) and O-acetylserine sulfhydrylase (OASS-A), the enzymes catalyzing the last two steps of cysteine biosynthesis, engage in the formation of the cysteine synthase (CS) complex. The interaction between SAT and OASS-A finely tunes cysteine homeostasis, and the development of inhibitors targeting either protein–protein interaction or the single enzymes represents an attractive strategy to undermine bacterial viability. Given the peculiar mode of interaction between SAT and OASS-A, which exploits the insertion of SAT C-terminal sequence into OASS-A active site, we tested whether a recently developed competitive inhibitor of OASS-A exhibited any effect on the CS stability. Through surface plasmon resonance spectroscopy, we (i) determined the equilibrium constant for the *Salmonella* Typhimurium CS complex formation and (ii) demonstrated that the inhibitor targeting OASS-A active site affects CS complex formation. For comparison, the *Escherichia coli* CS complex was also investigated, with the aim of testing the potential broad-spectrum activity of the candidate antimicrobial compound.

**Keywords:** cysteine synthase; cysteine biosynthesis; protein–protein interactions; competitive inhibitor; antibacterial; surface plasmon resonance; fluorescence

## 1. Introduction

Sulfur metabolism in bacteria supports the maintenance of intracellular redox homeostasis and takes part in the prevention of oxidative stress damages. Low molecular weight thiols as glutathione, mycothiol, bacillithiol, and coenzyme A efficiently buffer the reducing environment and are generally present at high concentrations to accomplish their function. Their synthesis primarily depends on the reservoir of cysteine which, in turn, can be stored as low molecular weight thiols. Indeed, cysteine is prone to autoxidation generating toxic reactive oxygen species, and the control of its biosynthesis and free concentration inside the cell is essential for bacterial fitness. The protection from oxidative stress is strictly related to the bacterial survival to host defenses and during latency stages, as well as to the contrast of antibiotics action [1–4]. Indeed, pathogen strains auxotroph for cysteine were found to be more susceptible to antibiotic administration being more exposed to oxidative

stress damages [5–8], which represents a common mechanism of action of large spectrum antibiotics. Therefore, in the compelling quest for effective antimicrobials able to counteract the ever-growing insurgence of resistances, cysteine biosynthesis has been individuated as a promising nonessential target for the development of antibiotic enhancers [9–13].

Most bacteria rely on the well-conserved reductive sulfate assimilation pathway for cysteine biosynthesis. The last two steps are catalyzed by serine acetyltransferase (SAT, EC 2.3.1.30) and *O*-acetylserine sulfhydrylase A (OASS-A, EC 2.5.1.47). SAT, a homo-hexameric enzyme, synthesizes *O*-acetylserine (OAS) in the presence of L-serine and acetyl coenzyme A, with OAS subsequently converted to L-cysteine by an OASS-A dimer in the presence of bisulfide. SAT and OASS-A engage in the formation of the multienzymatic complex cysteine synthase (CS), where a C-terminal tail of one subunit in each SAT trimer binds to one OASS-A active site and stabilizes the assembly, resulting in a 3:2 stoichiometry [14–18]. The activity of SAT is maximized when bound to OASS-A, while the latter is inhibited [17], although only a part of total OASS-A in the cell is involved in CS formation [19]. Even though the physiological function of CS has been only hypothetically assessed [20–22], it is well-established that its equilibrium is sensitive to the concentration of several metabolites, resulting in a fine-tuning of the two enzymatic activities. In fact, high concentrations of bisulfide stabilize CS complex [14], whereas OAS promotes its dissociation [14,23–25]; on the other hand, increasing levels of cysteine can inhibit SAT catalytic activity by feedback control, triggered by binding to its active site [26,27]. The alteration of this metabolic equilibrium can induce profound consequences in bacterial fitness, with several potential pleiotropic effects involving the numerous moonlighting functions of OASS-A [28–31].

In the last years, many efforts have been addressed to the development of potential inhibitors targeting cysteine pathway [32–34] and, in particular, OASS isoforms or SAT from several pathogen species [10,35–48]. A drug discovery campaign carried out in our laboratories led to the identification of the synthetic compound UPAR415 ((1*S*,2*S*)-1-(4-methylbenzyl)-2-phenylcyclopropanecarboxylic acid, Figure 1a) as the most potent inhibitor developed so far of OASS-A from *Salmonella* Typhimurium (StOASS-A), with a nanomolar dissociation constant for the target [41,49]. Microbiologic assays demonstrated a synergic and/or additive action of the compound with colistin, a last-line polycationic antibiotic, in several bacterial strains prone to the insurgence of antibiotic resistance. Target engagement experiments on *S. Typhimurium* cultures and cytotoxicity assays on eukaryotic cells, moreover, determined the inhibitor to be specific and nontoxic [49]. These data support the viability of the pursued approach and represent a good starting point for the development of a new class of antimicrobial compounds, targeting the enzymes of the sulfur reductive assimilation pathway. UPAR415, identified after several rounds of modification and selection of substituted cyclopropanes, is inspired to the C-terminal isoleucine of SAT, an extremely well-conserved residue responsible for CS anchorage [24,50]; because of its structure, this compound might destabilize the CS complex by competing with SAT tails for the occupation of OASS-A active site. Very recently, the pose of UPAR415 bound to StOASS-A was confirmed through crystallization studies (Figure 1, Protein Data Bank (PDB) id 6z4n, [49]). With this in mind, we decided to extend the mechanistic characterization of UPAR415 to a broader biochemical context, involving the engagement of OASS-A in the CS complex. The formation of the CS complex of *S. Typhimurium* has been herein investigated through surface plasmon resonance (SPR). The affinity between OASS-A and SAT, previously measured under conditions that partially destabilize the complex [51–53], was determined and found to be similar to that of the homologous complex from other Gammaproteobacteria, such as *Escherichia coli* and *Haemophilus influenzae*. The effects of UPAR415 on the formation of CS complex were then examined by exploiting SPR and static fluorescence experiments. Given the high sequence and structural homology of the constituent enzymes, the investigation was extended to the CS complex from *E. coli*, another emerging antibiotic-resistant bacterium for which innovative treatments are urgently required.

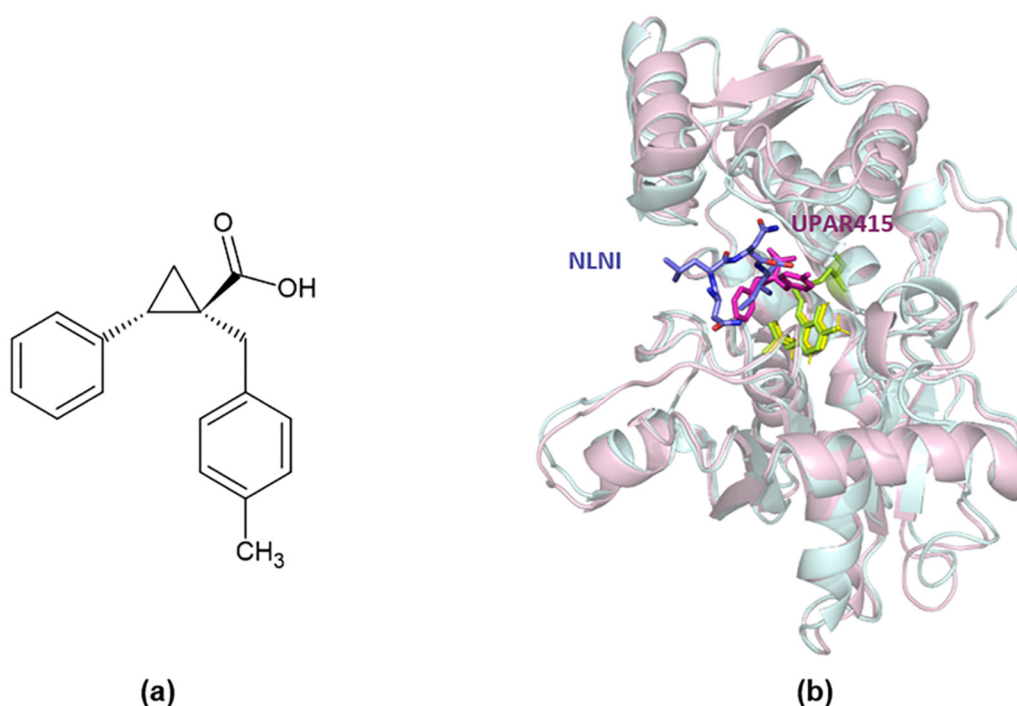


**Figure 1.** (a) UPAR415 ((1S,2S)-1-(4-methylbenzyl)-2-phenylcyclopropanecarboxylic acid) [41]. (b) superimposition of an StOASS-A monomer (light cyan) in complex with UPAR415 (magenta, PDB id 6z4n, [49]) and an OASS-A monomer from *H. influenzae* (light pink) in complex with the NLNI tetrapeptide (violet, PDB id 1y7l, [16]), representing the C-terminal sequence of SAT. UPAR415 is inspired to the C-terminal isoleucine residue, which is key for SAT binding to OASS-A and is conserved in the SAT sequences of *S. Typhimurium*, *E. coli*, and *H. influenzae*. The pyridoxal-5'-phosphate cofactor molecules are represented in yellow (StOASS-A) and green (HiOASS-A).

## 2. Results and Discussion

### 2.1. Determination of the Affinity of *Salmonella Typhimurium* Cysteine Synthase Complex

The formation of a cysteine synthase complex between OASS-A and SAT in *S. Typhimurium* and *E. coli* was first reported by Kredich and colleagues in the late 1960s [14,19,54,55], when serine transacetylase and *O*-acetylserine sulfhydrylase activities were co-purified, casting questions about the assembly composition, function, and dynamics. In the following decades, CS complexes were identified in other organisms, including bacteria, protozoa, and plants [16,56–59]. In this context, the engagement and the affinity of OASS-A and SAT in bacteria have been the object of several biophysical and kinetic studies, because of the potential pharmaceutical relevance of the cysteine biosynthetic pathway [15,17,24,31,52,60–63]. Studies on *S. Typhimurium* and *E. coli* are of particular relevance because of the inclusion of these two species in the global priority list of the World Health Organization for the insurgence of new antibiotic resistant [64].

Many studies describe the function and regulation of OASS-A and SAT from *E. coli* (EcOASS-A and EcSAT, respectively). Moreover, pre-steady state and SPR experiments allowed the determination of *E. coli* CS (EcCS) dissociation constant, found to be in the low nanomolar range [24,62]. On the other hand, despite the pioneering studies that led to the original discovery of the complex and the wealth of information available about the single proteins, the CS complex from *S. Typhimurium* (StCS) has been poorly investigated and several considerations reported in the literature are deduced by the high degree of similarity to the *E. coli* proteins (sequences identity >95%). Among the available data, SPR experiments carried out by Kaushik and colleagues on StCS indicate a  $K_D$  of 30–70 nM, also supported by other biophysical approaches [53]. This would indicate an affinity about an order of magnitude lower than that observed for the *E. coli* complex. These results, however, are likely affected by the experimental conditions: indeed, the chloride ions present in the

buffer at high concentration promote the transition of OASS-A to an inhibited conformation (PDB id 1fcj, [51]), thus affecting the formation of the complex [52].

To measure the affinity of the StCS complex by SPR, we exploited the immobilization of OASS-A by amine coupling on a CM5 golden chip. Increasing concentrations of StSAT (in the range of 0.5–50 nM) were sequentially injected and flushed on the chip at 25 °C to obtain a single-cycle kinetic sensorgram (Figure 2a). The data were fitted to the Langmuir 1:1 equation (see Materials and Methods), the simplest binding model, giving an equilibrium  $K_D$  for the complex formation of  $2.3 \pm 0.6$  nM. To validate our approach, the same experimental setup was applied for the determination of the affinity of the *E. coli* complex (Figure 3a). The calculated affinity at the equilibrium was  $2.3 \pm 0.1$  nM, in perfect agreement with the published data reported by other groups [24,62]. The analogy of the two constants, moreover, is in accordance with the high sequence and structural conservation of the partner proteins from *S. Typhimurium* and *E. coli*, and with the comparable tertiary conformations stabilized upon CS formations, that appears to favor an open-to-close rearrangement of both OASS-A subunits [18,65].

## 2.2. Interaction of UPAR415 and SAT with OASS-A

The structure of StOASS-A in complex with UPAR415 has been recently solved. The molecule accommodates in the enzyme active site and occupies, through its carboxylate moiety, the anchoring subsite of the C-terminal tail of SAT (Figure 1b, [16,49]). As demonstrated by the superimposition with the structure of *H. influenzae* OASS-A (HiOASS-A) bound to the SAT C-terminal decapeptide (PDB id 1y7l, [16]) or pentapeptides [36], the pose of UPAR415 mimics that of the C-terminal isoleucine residue. Due to the steric hindrance of the tolyl substituent, an evident closure movement is not elicited and OASS-A maintains a conformation similar to the one observed in the absence of ligands (PDB id 1oas, [65]). This narrow rearrangement also manifests upon peptides binding to HiOASS-A, which is unable to induce the large conformational changes that are assumed to take place upon full-length SAT binding, leading the transition to the closed conformation [18]; moreover, the peptides bind with much lower affinity to OASS-A (in the low micromolar range), supporting the existence of a more extended interaction network between SAT and OASS-A [36]. The indirect evidence of the different structural rearrangement upon binding of StSAT or UPAR415 is provided by static fluorescence measurements. OASS-A is a pyridoxal-5'-phosphate (PLP)-dependent enzyme and the cofactor can be exploited as an intrinsic probe to monitor the ligand binding to the active site of the enzyme, by changes in fluorescence intensity and emission wavelength [15,36,50,66]. Upon direct excitation of PLP at 412 nm, the emission signal of StOASS-A at 505 nm, in the absence of ligands, shifts to 502 nm in the presence of UPAR415 and 495 nm in the presence of StSAT, respectively (Figure 4a). These blue shifts may indicate the formation of a less polar environment within the active site, possibly associated with a closure or a rearrangement of the pocket leading to water exclusion, which is more pronounced in the case of SAT binding. The same emission behavior is displayed by EcOASS-A, and based on structural data, a comparable conformational change can be hypothesized (Figure 4b).

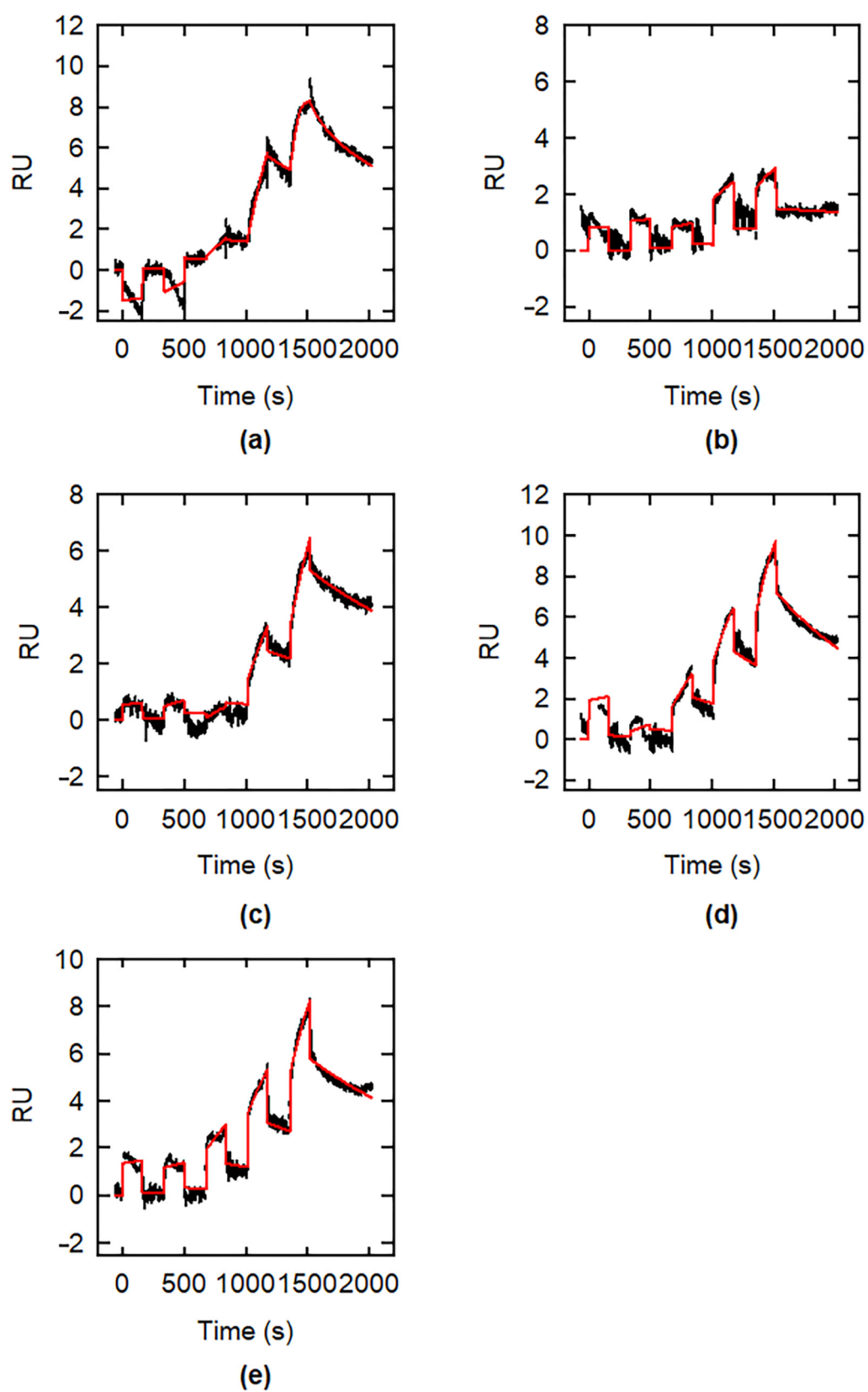


**Figure 2.** Kinetics of formation of StCS complex in the absence (a) and in the presence of 0.15  $\mu\text{M}$  (b), 0.3  $\mu\text{M}$  (c), 1  $\mu\text{M}$  (d) or 2  $\mu\text{M}$  (e) UPAR415. Data were fitted to the Langmuir 1:1 binding model (red lines). SAT was injected at five sequential concentrations of 0.5, 2.5, 5, 25, and 50 nM (a–c) or 2.5, 5, 25, 50, and 100 nM (d,e). Protein concentrations are expressed as monomers.

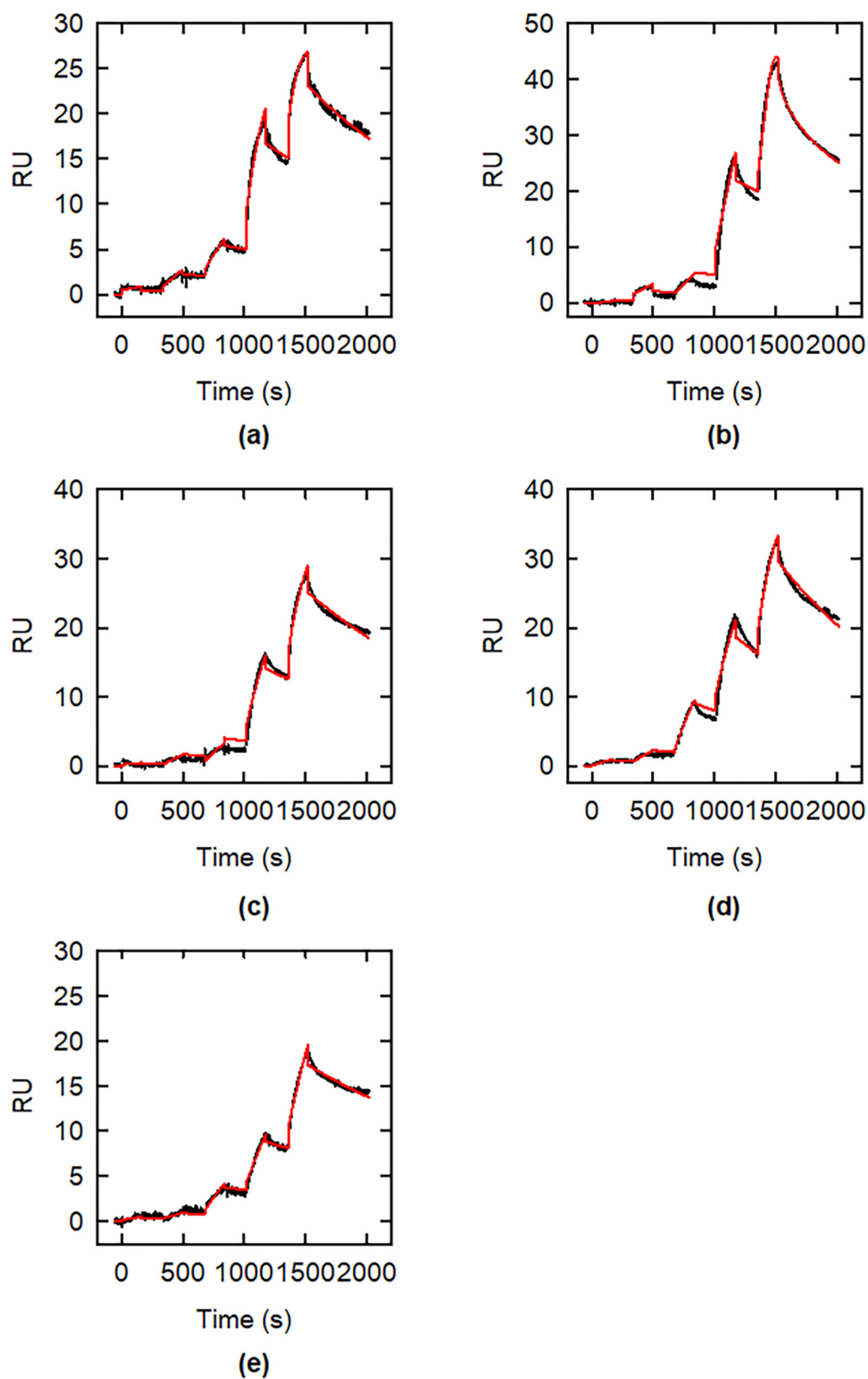


**Figure 3.** Kinetics of formation of EcCS complex in the absence (a) and in the presence of 0.15  $\mu\text{M}$  (b), 0.3  $\mu\text{M}$  (c), 1  $\mu\text{M}$  (d) or 2  $\mu\text{M}$  (e) UPAR415. Data were fitted to the Langmuir 1:1 binding model (red lines). SAT was injected at five sequential concentrations of 0.5, 2.5, 5, 25, and 50 nM (a–c) or 2.5, 5, 25, 50, and 100 nM (d,e). Protein concentrations are expressed as monomers.

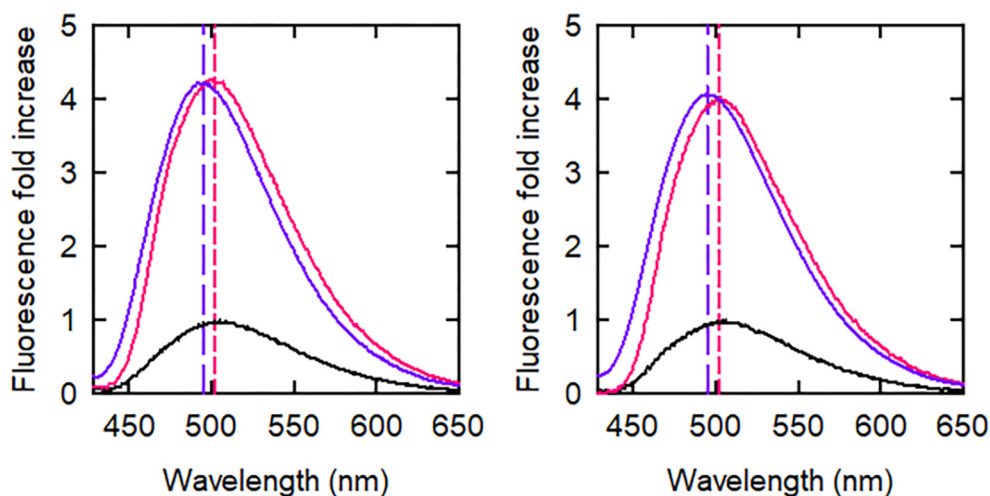


**Figure 4.** Changes in fluorescence emission spectra ( $\lambda_{\text{ex}} = 412 \text{ nm}$ ) of StOASS-A (a) or EcOASS-A (b) in the absence (black) and in the presence of saturating SAT (purple) or UPAR415 (pink). The peak is centered at 495 nm when CSC is formed and at 502 nm when the inhibitor is bound to OASS-A.

The fluorescence quantum yield increase upon UPAR415 binding was followed to determine the binding affinity for OASS-A. Previous studies reported the  $K_D$  of UPAR415 for StOASS-A at 20 °C ( $28 \pm 5 \text{ nM}$ , [41]); as a comparison, the constant for EcOASS-A was determined in the same experimental conditions ( $K_D = 48.3 \pm 6.2 \text{ nM}$ , data not shown) and was found to be in agreement with the values reported for the *S. Typhimurium* isoform. Because of the different temperature at which the SPR measurements have been carried out and the lack of binding experiments on EcOASS-A, we first determined the dissociation constants of UPAR415 for the two OASS-A orthologs at 25 °C (Figure 5). The calculated values for  $K_D$ s are  $97.3 \pm 6.3 \text{ nM}$  and  $55.8 \pm 8.0 \text{ nM}$  for the *S. Typhimurium* and the *E. coli* enzymes, respectively, indicating that the molecule, developed for StOASS-A inhibition, binds the *E. coli* isoform with a very similar affinity.

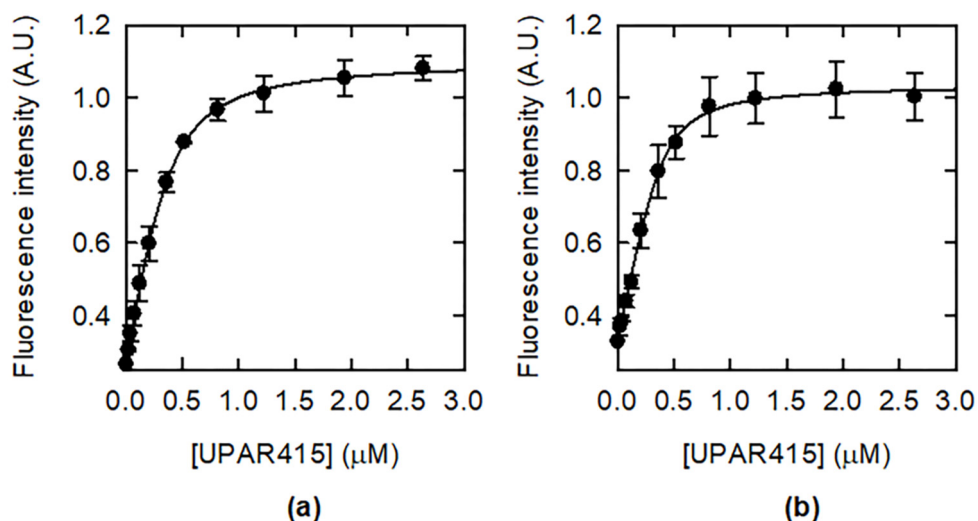


**Figure 5.** Binding of UPAR415 to StOASS-A (a) and EcOASS-A (b) at 25 °C. Fluorescence emission intensities at 500 nm upon excitation at 412 nm were fitted to a tight-binding equation (Equation (5)) giving  $K_D$  values of  $97.3 \pm 6.3 \text{ nM}$  for StOASS-A and  $55.8 \pm 8.0 \text{ nM}$  for EcOASS-A.

### 2.3. Effects of UPAR415 on CS Complex Formation

Following the same strategy exploited for the determination of the CS complex affinity, we moved to the SPR analysis of the effect of UPAR415 on the formation of the CS complex of both *S. Typhimurium* and *E. coli*. OASS-A was immobilized on the sensor chips and single-cycle kinetics were run by injecting increasing concentrations of SAT in the presence of a fixed concentration of UPAR415 per experiment (Figures 2b–e and 3b–e). These measurements allowed us to determine the CS complexes affinity decrease as induced by the inhibitor (Table 1). SAT and UPAR415 compete for the binding to OASS-A active site, and their concurrent presence reciprocally influences their apparent affinities for the target. Sensorgrams mirror the kinetics of SAT:OASS-A interaction, whose fitting to the Langmuir 1:1 binding model provides the apparent dissociation constant of CS complex as influenced by the different concentrations of UPAR415. Fitting of the sensorgrams reported in Figures 2 and 3 can also provide information on the kinetic parameters for complex formation and dissociation and how these are eventually influenced by UPAR415. However, CS formation, as reported for other bacterial species [31,52], is expected to be a complex, multistep process, and its accurate kinetic description is out of the scope of the present work.

**Table 1.** Comparison between experimental  $K_D$  of CS complex (CSC) from *S. Typhimurium* and *E. coli* in the presence of UPAR415 and predicted values obtained by Equation (4) (see Materials and Methods). The  $K_D$  values obtained by SPR measurements in the absence of inhibitor were used to calculate the predicted apparent dissociation constants. Errors are expressed as standard deviation.

[UPAR415] ( $\mu\text{M}$ )	Technique	Experimental $K_{D,app}$ CSC (nM)		Predicted $K_{D,app}$ CSC (nM)	
		<i>S. Typhimurium</i>	<i>E. coli</i>	<i>S. Typhimurium</i>	<i>E. coli</i>
0	SPR	$2.3 \pm 0.6$	$2.3 \pm 0.1$	-	-
0.15	SPR	$2.7 \pm 0.8$	$2.8 \pm 0.1$	3.4	3.9
0.3	SPR	$19.4 \pm 2.4$	$6.0 \pm 0.4$	4.5	5.5
1	SPR	$20.3 \pm 0.7$	$11.7 \pm 0.9$	9.7	13.0
2	SPR	$37.0 \pm 3.9$	$35.6 \pm 3.1$	17.0	23.7
2	Fluorescence	$59.2 \pm 4.2$	$69.1 \pm 8.6$	17.0	23.7
5	Fluorescence	$125.5 \pm 19.3$	$123.5 \pm 39.4$	39.1	55.8
10	Fluorescence	$253.7 \pm 50.8$	$269.2 \pm 53.5$	75.9	109.3

Concentrations of inhibitor above 2  $\mu\text{M}$  hampered the derivation of reliable SPR data since the apparent strength of the complexes is very likely out of the range of instrumental sensitivity (data not shown). We decided then to exploit static fluorescence experiments to investigate the behavior of the CS complexes at higher UPAR415 concentrations. Since the fluorescence quantum yield of the OASS-A:UPAR415 complex is similar to that obtained by the binding of SAT (Figure 4), the wavelength emission shifts were instead employed to monitor the displacement of the inhibitor from OASS-A active site by SAT. OASS-A was titrated with increasing concentrations of SAT in the presence of 2  $\mu\text{M}$ , 5  $\mu\text{M}$  or 10  $\mu\text{M}$  inhibitor (Figure 6) at 25 °C. Wavelength maxima shifts from 502 nm (OASS-A:UPAR415 complex) to 495 nm (OASS-A:SAT complex) were plotted against the SAT concentration and apparent  $K_D$  values were obtained by fitting data to a binding isotherm (Table 1). The 1:1 binding model applied to SPR data analysis allowed a direct comparison with static fluorescence data. Figure 7 reports the increase in the apparent dissociation constants of CS complex as a function of UPAR415 concentration. Lines represent the fitting of the data to Equation (4) (see Materials and Methods), rearranged to derive the apparent dissociation constant  $K_{D,app}$ . The intercept represents the  $K_D$  for CS complex (CSC) in the absence of inhibitor, whereas the slope corresponds to  $K_D \text{ CSC} / K_D \text{ U415}$  ratio. The linearity of the observed behavior confirms the complementarity of the data obtained through the two different approaches. The experimental point at 2  $\mu\text{M}$  UPAR415 was calculated both by SPR and static fluorescence measurements, further demonstrating a very good overlap of the results.

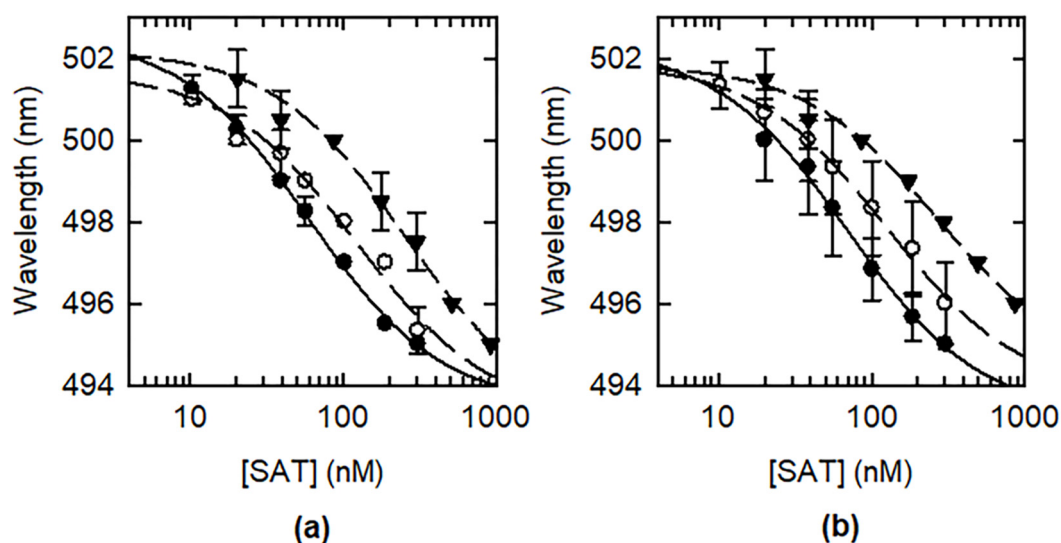


**Figure 6.** StCS (a) and EcCS (b) complex formation in the presence of 2  $\mu\text{M}$  (closed circles), 5  $\mu\text{M}$  (open circles) or 10  $\mu\text{M}$  (closed triangles) UPAR415. The displacement of UPAR415 by SAT from OASS-A active site is followed as wavelength shift as a function of SAT concentration. Data were fitted to a binding isotherm, giving the apparent  $K_D$  values reported in Table 1. Data represent the mean of technical triplicates and their standard deviations.

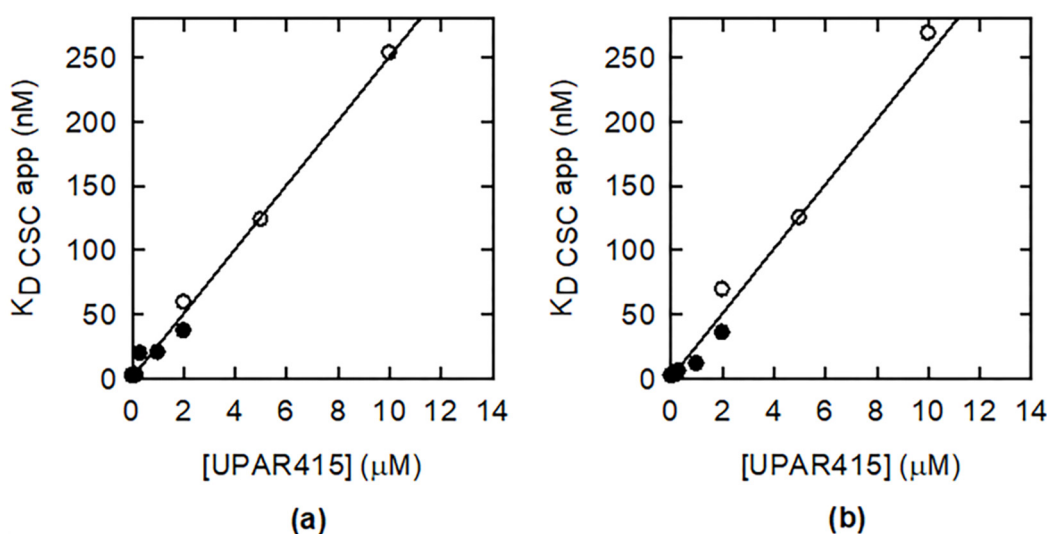


**Figure 7.** Apparent dissociation constants of StCS (a) and EcCS (b) complexes as a function of UPAR415 concentration, obtained by SPR single-cycle kinetics fitted to a 1:1 binding model (closed circles) and fluorescence titrations (open circles). Data were fitted to Equation (4) (see Materials and Methods, rearranged to derive the apparent dissociation constant  $K_{D,app}$ ) giving an offset of the order of  $10^{-9}$  M. This value, which represents extrapolated CS complex dissociation constants, is in good agreement with the independently determined values reported in Table 1 (2.3 nM for both CS complexes).

As can be noticed from data reported in Table 1 and Figure 7, UPAR415 elicits superimposable effects on the formation of StCS and EcCS complexes. Based on the increment of the retrieved apparent  $K_D$ s of CS complexes ( $K_{D,app}$  CSC, Table 1) in the presence of increasing concentrations of inhibitor, it is possible to observe that UPAR415 promotes the destabilization of the complexes formation by competing with SAT. Accordingly, when Equation (4) (see Materials and Methods), which assumes a simple competitive binding of two ligands for the same site, is applied to calculate the  $K_{D,app}$  from the  $K_D$ s of CS complexes in the absence of inhibitor, the theoretical values agree very well with the experimental results (Tables 1 and 2).

**Table 2.** CS complex dissociation constants obtained from the fitting with Equation (4) (Figure 7) of SPR and fluorescence data, corresponding to the  $K_{D,app}$  values for CS complex formation in the presence of increasing concentrations of UPAR415.

CS Complex	$K_D$ CSC (nM)	$K_D$ CSC/ $K_D$ UPAR415 (nM)	Extrapolated $K_D$ UPAR415 (nM)	$R^2$
<i>S. Typhimurium</i>	0.83	0.025	33.2	0.99
<i>E. coli</i>	0.63	0.025	25.2	0.95

As shown in Figure 7, the apparent  $K_D$ s were globally fitted to a linear equation (Equation (4)); the intercepts on the y-axes provided the theoretical affinity values for the formation of CS complex in the absence of inhibitor (0.83 nM for StCS and 0.63 nM for EcCS, Table 2), which are in agreement with the experimental data reported in Table 1. The ratios between the offsets on y-axes and the slopes of the fittings represent the  $K_D$ s of U415 for OASS-A (Table 2), giving a value of 33.2 nM for *S. Typhimurium* and 25.2 nM for *E. coli*, in good accordance with the  $K_D$  values determined by fluorescence measurements with the direct titrations (Figure 5).

### 3. Materials and Methods

#### 3.1. Chemicals and Reagents

All reagents were purchased from Merck (Darmstadt, Germany) and used as received, with the exception of acetyl coenzyme A, purchased from Applichem (Darmstadt, Germany).

#### 3.2. Expression and Purification of Recombinant Proteins

Recombinant proteins were independently overexpressed in *E. coli* host in LB medium in the presence of selective antibiotics and, in the case of SAT, of 2% glucose to promote mild induction conditions and hinder cysteine operon induction by *O*-acetylserine (OAS) accumulation. Cultures were grown at 37 °C under shaking until 0.5–0.6 OD was reached; isopropyl  $\beta$ -d-1-thiogalactopyranoside was then added to the medium at 1 mM final concentration, and cells were let grown under shaking for four hours. Cells were harvested by centrifugation, washed with phosphate-buffered saline solution, and stored as pellets at  $-80$  °C until further use. At the moment of purification, pellets were resuspended in lysis buffer (10 mL per gram of cells) in the presence of proteases inhibitors (1.5  $\mu$ M pepstatin A, 0.2 mM benzamidine, 0.2 mM phenylmethanesulfonyl fluoride), 1 mg/mL lysozyme and, in the case of OASS-A, 0.2 mM PLP. Cells were sonicated in ice by 10 s on/1 min off cycles, for 4 min. The supernatant containing the soluble proteins was separated from the cellular debris by centrifuging the samples at 16,000 g for 30 min. All the proteins were purified on an ÄKTA Prime (GE Healthcare, Uppsala, Sweden) FPLC system.

SAT from *S. Typhimurium* (StSAT) and *E. coli* (EcSAT) was expressed in BL21 Tuner™ (DE3) cells and purified as constructs presenting a His<sub>6</sub>-thioredoxin (TRX) tag at their N-termini, exploited to increase protein solubility and for IMAC purification on a Talon™ resin (Clontech Laboratories, Inc., Mountain View, CA, USA). Briefly, StSAT and EcSAT expressing cells were resuspended in buffer A (100 mM TRIS, 500 mM NaCl, 50 mM imidazole, 1 mM tricarboxyethyl phosphine (TCEP), 50  $\mu$ M L-cysteine, pH 7.5), in the presence of protease inhibitors and sonicated as described above. The supernatants were loaded on cobalt resin, previously equilibrated in buffer A, and the column was additionally washed to remove aspecific proteins. A solution of 10 mM OAS in buffer A, pH 7.0, was then flushed to remove endogenous bacterial OASS-A possibly bound to recombinant SAT to avoid the presence of contaminants in the final preparation. StSAT and EcSAT were finally eluted in the presence of 500 mM imidazole and fractions containing His-tagged TRX SAT were collected and put together in a 12 kDa-dialysis tube in the presence of 1 mM EDTA and 1 mM DTT. Then, 1 mg of in house produced His-tagged tobacco etch virus (TEV) protease every 50 mg of SAT was also added, to cut the His<sub>6</sub>-TRX tag. The solutions were dialyzed O/N against 20 mM TRIS, 250 mM NaCl, 1% glycerol, pH 7.5, and the following day they were recovered, centrifuged, and loaded on the Talon™ resin to

remove His<sub>6</sub>-TRX tags, uncleaved proteins, and TEV protease. The flow-through samples containing the purified SATs were then concentrated in an Amicon<sup>®</sup> stirred-cell (Merck-Millipore, Burlington, MA, USA), and the buffer was exchanged with 20 mM sodium phosphate, 250 mM NaCl, 2 mM EDTA, 10 mM 2-mercaptoethanol, pH 7.0. The proteins were loaded on a size-exclusion HiLoad 16/600 Superdex 75 prep grade column (GE Healthcare, Uppsala, Sweden); the final preparations were more than 95% pure based on the SDS-PAGE analysis.

OASS from *S. Typhimurium* (StOASS) was expressed in Rosetta<sup>™</sup> 2 (DE3) cells with an N-terminal His<sub>6</sub>-tag removable with TEV protease. Cells were lysed as described above in 50 mM sodium phosphate, 300 mM NaCl, pH 8.0, and the clarified supernatant was loaded on a Talon<sup>™</sup> resin; the column was washed in the presence of 20 mM imidazole and the protein was eluted with 300 mM imidazole. Fractions containing purified StOASS were collected and put together in a 12 kDa dialysis tube in the presence of 1 mM EDTA, fivefold molar excess of PLP, and 1 mg of TEV protease every 50 mg of protein. After O/N dialysis, the solution was recovered, centrifuged to remove precipitated proteins, and loaded again on the Talon<sup>™</sup> resin to separate cleaved tags, unreacted constructs and TEV protease. The final solution was concentrated and exchanged in 10 mM HEPES, 1 mM EDTA, 1 mM TCEP, pH 8.0.

OASS from *E. coli* (EcOASS) was expressed in Tuner<sup>™</sup> (DE3) cells with a C-terminal His<sub>10</sub>-tag. Cells were lysed as described above in 50 mM sodium phosphate, 300 mM NaCl, pH 7.0, and the clarified supernatant was loaded on a Talon<sup>™</sup> resin; the column was washed in the presence of 20 mM imidazole and the protein was eluted with 300 mM imidazole. Fractions containing purified EcOASS were collected and put together in a 12 kDa dialysis tube in the presence of 1 mM EDTA and a fivefold molar excess of PLP. After O/N dialysis, the solution was recovered, centrifuged to remove precipitated proteins and finally exchanged and concentrated in 10 mM HEPES, 1 mM EDTA, pH 8.0.

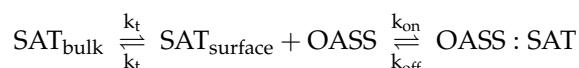
### 3.3. UPAR415

The synthesis and the characterization of UPAR415 (MW 266.34 g/mol) has been carried out as described in [41]. The powder was dissolved in 100% dimethyl sulfoxide (DMSO) to a 100 mM stock solution and then serially diluted in 100 mM HEPES, pH 7.0, and tested at the reported concentrations, containing a maximum of 0.01% DMSO, except if otherwise stated.

### 3.4. SPR Measurements

SPR single-cycle kinetics (SCK) measurements were performed at 25 °C by using a Biacore X100 instrument (GE Healthcare, Uppsala, Sweden). CM5 sensor chips and reagents were purchased from GE Healthcare, except HEPES buffer, supplied by Sigma-Aldrich (S. Louis, MO, USA). Experiments were carried out in 100 mM HEPES, pH 7.0, in the presence of 0.005% P20 surfactant, as running buffer. For each experiment, flow cell 1 (Fc1) was prepared as flow cell 2 (Fc2), but without intermediate ligand immobilization, and used as a reference for refractive index changes and nonspecific interactions. Before each SCK, the ligand OASS was covalently immobilized by amine coupling onto the Fc2 chip surface with a manual run setup. Briefly, the dextran matrix of the sensor chip was initially equilibrated with running buffer by three priming cycles of five minutes and its carboxyl groups were activated by flowing a solution of 0.1 M N-hydroxysuccinimide (NHS) and 0.4 M N-ethyl-N-(3-dimethylaminopropyl) carbodiimide (EDC) at 10 µL/min for 420 s. A solution of 11.5 µg/mL OASS in 10 mM acetate buffer, pH 5, was then injected at 10 µL/min for the coupling reaction. A final amount of ligand equal to 140–350 RU (resonance units) was immobilized on each sensor chip. Finally, 1 M ethanolamine hydrochloride, pH 8.5, was injected at 10 µL/min for 420 s over both Fc1 and Fc2, to block the unreacted groups. SCKs were carried out by the sequential injection of five increasing concentrations of the SAT analyte (range 0.5–100 nM, monomer concentration), without any regeneration step between consecutive injections [67]. For each injection step, SAT samples were fluxed

over the sensor chip surface for 160 s at 30  $\mu\text{L}/\text{min}$ , followed by a 500 s dissociation step with running buffer; at the end of the cycle, a final dissociation step of 400 s in running buffer was performed. SPR competition experiments in the presence of OASS inhibitor were carried out as described above, but for each SCK, injection samples were prepared in the presence of a fixed concentration of UPAR-415 (range 0.15–2  $\mu\text{M}$ ). SCK sensorgrams were globally fitted by using the Langmuir 1:1 binding model [68,69], assuming a simple reversible bimolecular reaction and considering the mass transport effect that drives the analyte toward the chip surface ( $\text{SAT}_{\text{surface}}$ ) or back to the bulk solution ( $\text{SAT}_{\text{bulk}}$ ), with the same mass transfer coefficient  $k_t$  [70]:



The binding of SAT to the ligand OASS-A brings to the formation of the CS complex, whose equilibrium depends on association ( $k_{\text{on}}$ ) and dissociation ( $k_{\text{off}}$ ) rate constants.

The temporal variation of analyte and ligand concentrations and of their complex was described by the following set of differential equations [71]:

$$d[\text{SAT}_{\text{surface}}]/dt = k_t([\text{SAT}_{\text{bulk}}] - [\text{SAT}_{\text{surface}}]) - (k_{\text{on}}[\text{OASS}][\text{SAT}_{\text{surface}}] - k_{\text{off}}[\text{OASS}:\text{SAT}]) \quad (1)$$

$$d[\text{OASS}]/dt = - (k_{\text{on}}[\text{OASS}][\text{SAT}_{\text{surface}}] - k_{\text{off}}[\text{OASS}:\text{SAT}]) \quad (2)$$

$$d[\text{OASS}:\text{SAT}]/dt = (k_{\text{on}}[\text{OASS}][\text{SAT}_{\text{surface}}] - k_{\text{off}}[\text{OASS}:\text{SAT}]) \quad (3)$$

The goodness of the fits was evaluated by  $\chi^2$  values and residual plots.

### 3.5. Fluorescence Measurements

Fluorescence binding experiments were performed on a Fluoromax-4 (Horiba Jobin-Yvon, Kyoto, Japan), or an FS5 (Edinburgh Instruments Ltd., Livingston, UK) spectrofluorometers equipped with a thermostated water bath. Measurements were carried out at 25  $^{\circ}\text{C}$  in a 3 mm pathlength quartz microcuvette in 100 mM HEPES buffer, pH 7.0. Before every experiment, proteins were spectrophotometrically quantified on a Cary 4000 spectrophotometer (Agilent, Santa Clara, CA, USA) by their extinction coefficients at 280 nm ( $\text{SAT}$ , *S. Typhimurium* 26930  $\text{M}^{-1} \text{cm}^{-1}$ ; *E. coli* 26930  $\text{M}^{-1} \text{cm}^{-1}$ ), determined by ProtParam software [72] or 412 nm (OASS-A), corresponding to the internal aldimine maximum emission wavelength (*S. Typhimurium* 9040  $\text{M}^{-1} \text{cm}^{-1}$ ; *E. coli* 9375  $\text{M}^{-1} \text{cm}^{-1}$  [31]). OASS-A solutions (100 nM) were titrated with increasing amounts of SAT in the presence of a fixed concentration of UPAR415 inhibitor (0.5, 5, or 10  $\mu\text{M}$ ). After each addition of SAT, the solution was incubated for 2 min to equilibrate the complex formation. The blue shift related to UPAR415 displacement from OASS active site by SAT was followed by collecting emission spectra upon PLP excitation at 412 nm.

Emission wavelength maxima were fitted to a binding isotherm to determine the apparent dissociation constant  $K_{\text{D,app}}$  of CS complex [73]. The intrinsic dissociation constant is obtained by the equation:

$$K_{\text{D}} = \frac{K_{\text{D,app}}}{1 + \frac{[\text{I}]}{K_{\text{D,I}}}} \quad (4)$$

where L is represented by UPAR415 and  $K_{\text{D,L}}$  is its dissociation constant at 25  $^{\circ}\text{C}$ .

The dissociation constants of UPAR415 for OASS-A were determined in 100 mM HEPES buffer, pH 7.0, in the presence of 5% DMSO. Emission spectra upon excitation at 412 nm of solutions containing 365 nM StOASS-A or 385 nM EcOASS-A in the presence of increasing concentrations of UPAR415 were collected, and fluorescence intensities at 500 nm were plotted to inhibitor concentration. Data were fitted to a quadratic equation describing tight binding:

$$I = I_0 + a \times \frac{[\text{OASS} - \text{A}] + [\text{U415}] + K_D - \sqrt{([\text{OASS} - \text{A}] + [\text{U415}] + K_D)^2 - (4 \times [\text{OASS} - \text{A}] \times [\text{U415}])}}{2} \quad (5)$$

where  $I$  is the fluorescence intensity at 500 nm,  $I_0$  is a horizontal offset,  $a$  is the maximum change in fluorescence at saturating ligand, and  $K_D$  is the dissociation constant of OASS-A:UPAR415 complex.

#### 4. Conclusions

The rapid spreading of bacterial resistances urges the search of novel antimicrobial compounds and antibiotic adjuvants. In this context, the metabolism of cysteine represents an attractive and promising target to undermine bacterial abilities of adaptation. Indeed, the reducing properties of cysteine are employed as an effective response to the oxidative stress experimented by bacteria during persistence phases in the host and induced by antibiotics. Several studies have illustrated the upregulation of different genes of cysteine metabolism and, on the other hand, an increased susceptibility to antimicrobial agents of strains characterized by an impaired oxidative stress response [3,7,8,74]. In this framework, in the last years, cysteine biosynthetic pathway has been the object of several drug discovery campaigns. A particular attention has been addressed to SAT and OASS-A, the two enzymes catalyzing the last two steps in cysteine biosynthesis in bacteria. SAT and OASS-A can assemble in a finely regulated bi-enzymatic complex known as cysteine synthase (CS), whose formation and regulation affect the single enzyme activities and finely tune many aspects of bacterial fitness and responses to external stimuli, comprising defense and protection mechanisms. In this context, a recent drug discovery campaign individuated the molecule UPAR415 as the most potent synthetic inhibitor for OASS-A developed so far. Recently, we demonstrated the viability of targeting OASS-A, showing through microbiological studies that the inhibition of this enzyme has synergic or additive effects with the last-line antibiotic colistin. Besides these results and the previous biochemical studies *in vitro* on OASS-A [41], the broader impact of UPAR415 on cysteine metabolism has to be further investigated. In this work, we exploited surface plasmon resonance and static fluorescence measurements to analyze the influence of UPAR415 on the complex formation between SAT and OASS-A from *S. Typhimurium* and *E. coli*. Experimental results demonstrated the ability of the inhibitor, initially developed for *S. Typhimurium* OASS-A inhibition, to decrease the apparent affinity of the CS complex of both bacteria by interfering with SAT binding to OASS-A active site. This effect could impact the action of SAT *in vivo*, whose activity is maximized when bound to OASS-A, thus limiting the supply of OAS and altering the regulation of cysteine regulon. Indeed, it has been reported that mutations of SAT that affect CS complex formation exert pleiotropic effects on OASS-A activity, resulting in cysteine auxotrophy [28]. This study paves the way for a deeper understanding of the effect of OASS inhibitors on the activity and regulation of cysteine biosynthetic pathway *in vivo*. In perspective, an updated knowledge of the inhibition mechanisms of OASS and SAT might guide the design of more potent compounds, susceptible to impact not only the synthesis of cysteine but also the full range of regulatory activities related to CS complex.

**Author Contributions:** Conceptualization, S.B., B.C., S.C., A.R.B. and A.M.; formal analysis, M.M. and F.S.D.A.; investigation, M.M., F.S.D.A., L.R., G.A. and M.P.; resources, G.C., S.B. and S.C.; writing—original draft preparation, M.M.; visualization, M.M.; supervision, S.B., B.C., S.C. and A.R.B.; funding acquisition, S.B., B.C., G.C. and S.C. All authors have read and agreed to the published version of the manuscript.

**Funding:** This research was funded by University of Parma research grants (to S.B., B.C. and G.C.).

**Acknowledgments:** Thanks are due to A.F. Montanarella for preliminary SPR experiments.

**Conflicts of Interest:** The authors declare no conflict of interest.

## References

1. Rengarajan, J.; Bloom, B.R.; Rubin, E.J. Genome-wide requirements for *Mycobacterium tuberculosis* adaptation and survival in macrophages. *Proc. Natl. Acad. Sci. USA* **2005**, *102*, 8327–8332. [[CrossRef](#)]
2. Hassett, D.J.; Imlay, J.A. Bactericidal Antibiotics and Oxidative Stress: A Radical Proposal. *ACS Chem. Biol.* **2007**, *2*, 708–710. [[CrossRef](#)] [[PubMed](#)]
3. Kohanski, M.A.; Dwyer, D.J.; Hayete, B.; Lawrence, C.A.; Collins, J.J. A Common Mechanism of Cellular Death Induced by Bactericidal Antibiotics. *Cell* **2007**, *130*, 797–810. [[CrossRef](#)] [[PubMed](#)]
4. Fox, D.T.; Schmidt, E.N.; Tian, H.; Dhungana, S.; Valentine, M.C.; Warrington, N.V.; Phillips, P.D.; Finney, K.B.; Cope, E.K.; Leid, J.G.; et al. Sub-Inhibitory Fosmidomycin Exposures Elicits Oxidative Stress in *Salmonella enterica* Serovar *typhimurium* LT2. *PLoS ONE* **2014**, *9*, e95271. [[CrossRef](#)]
5. Oppezzo, O.J.; Antón, D.N. Involvement of *cysB* and *cysE* genes in the sensitivity of *Salmonella typhimurium* to *mecillinam*. *J. Bacteriol.* **1995**, *177*, 4524–4527. [[CrossRef](#)]
6. Senaratne, R.H.; De Silva, A.D.; Williams, S.J.; Mougous, J.D.; Reader, J.R.; Zhang, T.; Chan, S.; Sidders, B.; Lee, D.H.; Chan, J.; et al. 5'-Adenosinephosphosulphate reductase (CysH) protects *Mycobacterium tuberculosis* against free radicals during chronic infection phase in mice. *Mol. Microbiol.* **2006**, *59*, 1744–1753. [[CrossRef](#)] [[PubMed](#)]
7. Turnbull, A.L.; Surette, M.G. L-Cysteine is required for induced antibiotic resistance in actively swarming *Salmonella enterica* serovar *Typhimurium*. *Microbiology* **2008**, *154*, 3410–3419. [[CrossRef](#)]
8. Turnbull, A.L.; Surette, M.G. Cysteine biosynthesis, oxidative stress and antibiotic resistance in *Salmonella typhimurium*. *Res. Microbiol.* **2010**, *161*, 643–650. [[CrossRef](#)]
9. Becker, D.; Selbach, M.; Rollenhagen, C.; Ballmaier, M.; Meyer, T.F.; Mann, M.; Bumann, D. Robust *Salmonella* metabolism limits possibilities for new antimicrobials. *Nature* **2006**, *440*, 303–307. [[CrossRef](#)]
10. Jean Kumar, V.U.; Poyraz, Ö.; Saxena, S.; Schnell, R.; Yogeeswari, P.; Schneider, G.; Sriram, D. Discovery of novel inhibitors targeting the *Mycobacterium tuberculosis* O-acetylserine sulphydrylase (CysK1) using virtual high-throughput screening. *Bioorg. Med. Chem. Lett.* **2013**, *23*, 1182–1186. [[CrossRef](#)]
11. Campanini, B.; Pieroni, M.; Raboni, S.; Bettati, S.; Benoni, R.; Pecchini, C.; Costantino, G.; Mozzarelli, A. Inhibitors of the sulfur assimilation pathway in bacterial pathogens as enhancers of antibiotic therapy. *Curr. Med. Chem.* **2015**, *22*, 187–213. [[CrossRef](#)]
12. Hicks, J.L.; Mullholland, C.V. Cysteine biosynthesis in *Neisseria* species. *Microbiology* **2018**, *164*, 1471–1480. [[CrossRef](#)]
13. Annunziato, G. Strategies to Overcome Antimicrobial Resistance (AMR) Making Use of Non-Essential Target Inhibitors: A Review. *Int. J. Mol. Sci.* **2019**, *20*, 5844. [[CrossRef](#)] [[PubMed](#)]
14. Kredich, N.M.; Becker, M.A.; Tomkins, G.M. Purification and characterization of cysteine synthetase, a bifunctional protein complex, from *Salmonella typhimurium*. *J. Biol. Chem.* **1969**, *244*, 2428–2439. [[CrossRef](#)]
15. Campanini, B.; Speroni, F.; Salsi, E.; Cook, P.F.; Roderick, S.L.; Huang, B.; Bettati, S.; Mozzarelli, A. Interaction of serine acetyltransferase with O-acetylserine sulphydrylase active site: Evidence from fluorescence spectroscopy. *Protein Sci.* **2005**, *14*, 2115–2124. [[CrossRef](#)]
16. Huang, B.; Vetting, M.W.; Roderick, S.L. The Active Site of O-Acetylserine Sulphydrylase Is the Anchor Point for Bienzyme Complex Formation with Serine Acetyltransferase. *J. Bacteriol.* **2005**, *187*, 3201–3205. [[CrossRef](#)] [[PubMed](#)]
17. Benoni, R.; De Bei, O.; Paredi, G.; Hayes, C.S.; Franko, N.; Mozzarelli, A.; Bettati, S.; Campanini, B. Modulation of *Escherichia coli* serine acetyltransferase catalytic activity in the cysteine synthase complex. *FEBS Lett.* **2017**, *591*, 1212–1224. [[CrossRef](#)]
18. Rosa, B.; Marchetti, M.; Paredi, G.; Amenitsch, H.; Franko, N.; Benoni, R.; Giabbai, B.; De Marino, M.G.; Mozzarelli, A.; Ronda, L.; et al. Combination of SAXS and Protein Painting Discloses the Three-Dimensional Organization of the Bacterial Cysteine Synthase Complex, a Potential Target for Enhancers of Antibiotic Action. *Int. J. Mol. Sci.* **2019**, *20*, 5219. [[CrossRef](#)]
19. Kredich, N.M.; Tomkins, G.M. The Biosynthesis of L-Cysteine in *Escherichia coli* and *Salmonella typhimurium* by a Multifunctional Enzyme Complex. In *Organizational Biosynthesis*; Vogel, H.J., Lampen, J.O., Bryson, V., Eds.; Academic Press: Cambridge, MA, USA, 1967; pp. 189–198.
20. Droux, M.; Ruffet, M.L.; Douce, R.; Job, D. Interactions between serine acetyltransferase and O-acetylserine (thiol) lyase in higher plants—structural and kinetic properties of the free and bound enzymes. *Eur. J. Biochem.* **1998**, *255*, 235–245. [[CrossRef](#)]
21. Mino, K.; Imamura, K.; Sakiyama, T.; Eisaki, N.; Matsuyama, A.; Nakanishi, K. Increase in the stability of serine acetyltransferase from *Escherichia coli* against cold inactivation and proteolysis by forming a bienzyme complex. *Biosci. Biotechnol. Biochem.* **2001**, *65*, 865–874. [[CrossRef](#)] [[PubMed](#)]
22. Yi, H.; Dey, S.; Kumaran, S.; Lee, S.G.; Krishnan, H.B.; Jez, J.M. Structure of Soybean Serine Acetyltransferase and Formation of the Cysteine Regulatory Complex as a Molecular Chaperone\*. *J. Biol. Chem.* **2013**, *288*, 36463–36472. [[CrossRef](#)] [[PubMed](#)]
23. Berkowitz, O.; Wirtz, M.; Wolf, A.; Kuhlmann, J.; Hell, R. Use of biomolecular interaction analysis to elucidate the regulatory mechanism of the cysteine synthase complex from *Arabidopsis thaliana*. *J. Biol. Chem.* **2002**, *277*, 30629–30634. [[CrossRef](#)] [[PubMed](#)]
24. Zhao, C.; Moriga, Y.; Feng, B.; Kumada, Y.; Imanaka, H.; Imamura, K.; Nakanishi, K. On the interaction site of serine acetyltransferase in the cysteine synthase complex from *Escherichia coli*. *Biochem. Biophys. Res. Commun.* **2006**, *341*, 911–916. [[CrossRef](#)]
25. Schnell, R.; Oehlmann, W.; Singh, M.; Schneider, G. Structural insights into catalysis and inhibition of O-acetylserine sulphydrylase from *Mycobacterium tuberculosis*. Crystal structures of the enzyme alpha-aminoacrylate intermediate and an enzyme-inhibitor complex. *J. Biol. Chem.* **2007**, *282*, 23473–23481. [[CrossRef](#)]

26. Hindson, V.J. Serine acetyltransferase of *Escherichia coli*: Substrate specificity and feedback control by cysteine. *Biochem. J.* **2003**, *375*, 745–752. [[CrossRef](#)]
27. Olsen, L.R.; Huang, B.; Vetting, M.W.; Roderick, S.L. Structure of serine acetyltransferase in complexes with CoA and its cysteine feedback inhibitor. *Biochemistry* **2004**, *43*, 6013–6019. [[CrossRef](#)]
28. Becker, M.A.; Tomkins, G.M. Pleiotrophy in a cysteine-requiring mutant of *Salmonella typhimurium* resulting from altered protein-protein interaction. *J. Biol. Chem.* **1969**, *244*, 6023–6030. [[CrossRef](#)]
29. Sturgill, G.; Toutain, C.M.; Komperda, J.; O'Toole, G.A.; Rather, P.N. Role of CysE in Production of an Extracellular Signaling Molecule in *Providencia stuartii* and *Escherichia coli*: Loss of *cysE* Enhances Biofilm Formation in *Escherichia coli*. *J. Bacteriol.* **2004**, *186*, 7610–7617. [[CrossRef](#)]
30. Campanini, B.; Benoni, R.; Bettati, S.; Beck, C.M.; Hayes, C.S.; Mozzarelli, A. Moonlighting O-acetylserine sulfhydrylase: New functions for an old protein. *Biochim. Biophys. Acta* **2015**, *1854*, 1184–1193. [[CrossRef](#)]
31. Benoni, R.; Beck, C.M.; Garza-Sánchez, F.; Bettati, S.; Mozzarelli, A.; Hayes, C.S.; Campanini, B. Activation of an anti-bacterial toxin by the biosynthetic enzyme CysK: Mechanism of binding, interaction specificity and competition with cysteine synthase. *Sci. Rep.* **2017**, *7*, 8817. [[CrossRef](#)] [[PubMed](#)]
32. Jez, J.M.; Dey, S. The cysteine regulatory complex from plants and microbes: What was old is new again. *Curr. Opin. Struct. Biol.* **2013**, *23*, 302–310. [[CrossRef](#)]
33. Palde, P.B.; Bhaskar, A.; Pedró Rosa, L.E.; Madoux, F.; Chase, P.; Gupta, V.; Spicer, T.; Scampavia, L.; Singh, A.; Carroll, K.S. First-in-Class Inhibitors of Sulfur Metabolism with Bactericidal Activity against Non-Replicating *M. tuberculosis*. *ACS Chem. Biol.* **2016**, *11*, 172–184. [[CrossRef](#)] [[PubMed](#)]
34. Mori, M.; Tsuge, S.; Fukasawa, W.; Jeelani, G.; Nakada-Tsukui, K.; Nonaka, K.; Matsumoto, A.; Ōmura, S.; Nozaki, T.; Shiomi, K. Discovery of Antiamebic Compounds That Inhibit Cysteine Synthase from the Enteric Parasitic Protist *Entamoeba histolytica* by Screening of Microbial Secondary Metabolites. *Front. Cell. Infect. Microbiol.* **2018**, *8*. [[CrossRef](#)]
35. Agarwal, S.M.; Jain, R.; Bhattacharya, A.; Azam, A. Inhibitors of *Escherichia coli* serine acetyltransferase block proliferation of *Entamoeba histolytica* trophozoites. *Int. J. Parasitol.* **2008**, *38*, 137–141. [[CrossRef](#)]
36. Salsi, E.; Bayden, A.S.; Spyraakis, F.; Amadasi, A.; Campanini, B.; Bettati, S.; Dodatko, T.; Cozzini, P.; Kellogg, G.E.; Cook, P.F.; et al. Design of O-acetylserine sulfhydrylase inhibitors by mimicking nature. *J. Med. Chem.* **2010**, *53*, 345–356. [[CrossRef](#)]
37. Amori, L.; Katkevica, S.; Bruno, A.; Campanini, B.; Felici, P.; Mozzarelli, A.; Costantino, G. Design and synthesis of trans-2-substituted-cyclopropane-1-carboxylic acids as the first non-natural small molecule inhibitors of O-acetylserine sulfhydrylase. *MedChemComm* **2012**, *3*, 1111–1116. [[CrossRef](#)]
38. Nagpal, I.; Raj, I.; Subbarao, N.; Gourinath, S. Virtual Screening, Identification and In Vitro Testing of Novel Inhibitors of O-Acetyl-L-Serine Sulfhydrylase of *Entamoeba histolytica*. *PLoS ONE* **2012**, *7*, e30305. [[CrossRef](#)] [[PubMed](#)]
39. Spyraakis, F.; Singh, R.; Cozzini, P.; Campanini, B.; Salsi, E.; Felici, P.; Raboni, S.; Benedetti, P.; Cruciani, G.; Kellogg, G.E.; et al. Isozyme-Specific Ligands for O-acetylserine sulfhydrylase, a Novel Antibiotic Target. *PLoS ONE* **2013**, *8*, e77558. [[CrossRef](#)]
40. Brunner, K.; Maric, S.; Reshma, R.S.; Almqvist, H.; Seashore-Ludlow, B.; Gustavsson, A.-L.; Poyraz, Ö.; Yogeewari, P.; Lundbäck, T.; Vallin, M.; et al. Inhibitors of the Cysteine Synthase CysM with Antibacterial Potency against Dormant *Mycobacterium tuberculosis*. *J. Med. Chem.* **2016**, *59*, 6848–6859. [[CrossRef](#)]
41. Pieroni, M.; Annunziato, G.; Beato, C.; Wouters, R.; Benoni, R.; Campanini, B.; Pertinhez, T.A.; Bettati, S.; Mozzarelli, A.; Costantino, G. Rational Design, Synthesis, and Preliminary Structure-Activity Relationships of  $\alpha$ -Substituted-2-Phenylcyclopropane Carboxylic Acids as Inhibitors of *Salmonella typhimurium* O-Acetylserine Sulfhydrylase. *J. Med. Chem.* **2016**, *59*, 2567–2578. [[CrossRef](#)]
42. Brunner, K.; Steiner, E.M.; Reshma, R.S.; Sriram, D.; Schnell, R.; Schneider, G. Profiling of in vitro activities of urea-based inhibitors against cysteine synthases from *Mycobacterium tuberculosis*. *Bioorganic Med. Chem. Lett.* **2017**, *27*, 4582–4587. [[CrossRef](#)]
43. Franko, N.; Grammatoglou, K.; Campanini, B.; Costantino, G.; Jirgensons, A.; Mozzarelli, A. Inhibition of O-acetylserine sulfhydrylase by fluoroalanine derivatives. *J. Enzym. Inhib. Med. Chem.* **2018**, *33*, 1343–1351. [[CrossRef](#)]
44. Magalhães, J.; Franko, N.; Annunziato, G.; Welch, M.; Dolan, S.K.; Bruno, A.; Mozzarelli, A.; Armao, S.; Jirgensons, A.; Pieroni, M.; et al. Discovery of novel fragments inhibiting O-acetylserine sulphhydrylase by combining scaffold hopping and ligand-based drug design. *J. Enzym. Inhib. Med. Chem.* **2018**, *33*, 1444–1452. [[CrossRef](#)] [[PubMed](#)]
45. Magalhães, J.; Franko, N.; Annunziato, G.; Pieroni, M.; Benoni, R.; Nikitjuka, A.; Mozzarelli, A.; Bettati, S.; Karawajczyk, A.; Jirgensons, A.; et al. Refining the structure-activity relationships of 2-phenylcyclopropane carboxylic acids as inhibitors of O-acetylserine sulfhydrylase isoforms. *J. Enzym. Inhib. Med. Chem.* **2019**, *34*, 31–43. [[CrossRef](#)]
46. Magalhães, J.; Franko, N.; Raboni, S.; Annunziato, G.; Tammela, P.; Bruno, A.; Bettati, S.; Mozzarelli, A.; Pieroni, M.; Campanini, B.; et al. Inhibition of Nonessential Bacterial Targets: Discovery of a Novel Serine O-Acetyltransferase Inhibitor. *ACS Med. Chem. Lett.* **2020**, *11*, 790–797. [[CrossRef](#)] [[PubMed](#)]
47. Wallace, M.J.; Dharuman, S.; Fernando, D.M.; Reeve, S.M.; Gee, C.T.; Yao, J.; Griffith, E.C.; Phelps, G.A.; Wright, W.C.; Elmore, J.M.; et al. Discovery and Characterization of the Antimetabolite Action of Thioacetamide-Linked 1,2,3-Triazoles as Disruptors of Cysteine Biosynthesis in Gram-Negative Bacteria. *ACS Infect. Dis.* **2020**, *6*, 467–478. [[CrossRef](#)] [[PubMed](#)]
48. Magalhães, J.; Franko, N.; Raboni, S.; Annunziato, G.; Tammela, P.; Bruno, A.; Bettati, S.; Armao, S.; Spadini, C.; Cabassi, C.S.; et al. Discovery of Substituted (2-Aminooxazol-4-yl)isoxazole-3-carboxylic Acids as Inhibitors of Bacterial Serine Acetyltransferase in the Quest for Novel Potential Antibacterial Adjuvants. *Pharmaceuticals* **2021**, *14*, 174. [[CrossRef](#)]

49. Annunziato, G.; Spadini, C.; Franko, N.; Storici, P.; Demitri, N.; Pieroni, M.; Flisi, S.; Rosati, L.; Iannarelli, M.; Marchetti, M.; et al. Investigational Studies on a Hit Compound Cyclopropane-Carboxylic Acid Derivative Targeting O-Acetylserine Sulfhydrylase as a Colistin Adjuvant. *ACS Infect. Dis.* **2021**, *7*, 281–292. [[CrossRef](#)]
50. Spyrakakis, F.; Felici, P.; Bayden, A.S.; Salsi, E.; Miggiano, R.; Kellogg, G.E.; Cozzini, P.; Cook, P.F.; Mozzarelli, A.; Campanini, B. Fine tuning of the active site modulates specificity in the interaction of O-acetylserine sulfhydrylase isozymes with serine acetyltransferase. *Biochim. Biophys. Acta* **2013**, *1834*, 169–181. [[CrossRef](#)]
51. Burkhard, P.; Tai, C.H.; Jansonius, J.N.; Cook, P.F. Identification of an allosteric anion-binding site on O-acetylserine sulfhydrylase: Structure of the enzyme with chloride bound. *J. Mol. Biol.* **2000**, *303*, 279–286. [[CrossRef](#)]
52. Salsi, E.; Campanini, B.; Bettati, S.; Raboni, S.; Roderick, S.L.; Cook, P.F.; Mozzarelli, A. A Two-step Process Controls the Formation of the Bienzyme Cysteine Synthase Complex\*. *J. Biol. Chem.* **2010**, *285*, 12813–12822. [[CrossRef](#)] [[PubMed](#)]
53. Kaushik, A.; Ekka, M.K.; Kumaran, S. Two Distinct Assembly States of the Cysteine Regulatory Complex of *Salmonella typhimurium* Are Regulated by Enzyme–Substrate Cognate Pairs. *Biochemistry* **2017**, *56*, 2385–2399. [[CrossRef](#)]
54. Kredich, N.M.; Tomkins, G.M. The enzymic synthesis of L-cysteine in *Escherichia coli* and *Salmonella typhimurium*. *J. Biol. Chem.* **1966**, *241*, 4955–4965. [[CrossRef](#)]
55. Becker, M.A.; Kredich, N.M.; Tomkins, G.M. The Purification and Characterization of O-Acetylserine Sulfhydrylase-A from *Salmonella typhimurium*. *J. Biol. Chem.* **1969**, *244*, 2418–2427. [[CrossRef](#)]
56. Wirtz, M.; Berkowitz, O.; Droux, M.; Hell, R. The cysteine synthase complex from plants. Mitochondrial serine acetyltransferase from *Arabidopsis thaliana* carries a bifunctional domain for catalysis and protein-protein interaction. *Eur. J. Biochem.* **2001**, *268*, 686–693. [[CrossRef](#)]
57. Bonner, E.R.; Cahoon, R.E.; Knapke, S.M.; Jez, J.M. Molecular basis of cysteine biosynthesis in plants: Structural and functional analysis of O-acetylserine sulfhydrylase from *Arabidopsis thaliana*. *J. Biol. Chem.* **2005**, *280*, 38803–38813. [[CrossRef](#)] [[PubMed](#)]
58. Francois, J.A.; Kumaran, S.; Jez, J.M. Structural basis for interaction of O-acetylserine sulfhydrylase and serine acetyltransferase in the *Arabidopsis* cysteine synthase complex. *Plant Cell* **2006**, *18*, 3647–3655. [[CrossRef](#)]
59. Raj, I.; Kumar, S.; Gourinath, S. The narrow active-site cleft of O-acetylserine sulfhydrylase from *Leishmania donovani* allows complex formation with serine acetyltransferases with a range of C-terminal sequences. *Acta Crystallogr. D Biol. Crystallogr.* **2012**, *68*, 909–919. [[CrossRef](#)]
60. Cook, P.F.; Wedding, R.T. Initial kinetic characterization of the multienzyme complex, cysteine synthetase. *Arch. Biochem. Biophys.* **1977**, *178*, 293–302. [[CrossRef](#)]
61. Mino, K.; Yamanoue, T.; Sakiyama, T.; Eisaki, N.; Matsuyama, A.; Nakanishi, K. Effects of Bienzyme Complex Formation of Cysteine Synthetase from *Escherichia coli* on Some Properties and Kinetics. *Biosci. Biotechnol. Biochem.* **2000**, *64*, 1628–1640. [[CrossRef](#)] [[PubMed](#)]
62. Wang, T.; Leyh, T.S. Three-stage assembly of the cysteine synthase complex from *Escherichia coli*. *J. Biol. Chem.* **2012**, *287*, 4360–4367. [[CrossRef](#)]
63. Dharavath, S.; Raj, I.; Gourinath, S. Structure-based mutational studies of O-acetylserine sulfhydrylase reveal the reason for the loss of cysteine synthase complex formation in *Brucella abortus*. *Biochem. J.* **2017**, *474*, 1221–1239. [[CrossRef](#)] [[PubMed](#)]
64. Tacconelli, E.; Carrara, E.; Savoldi, A.; Harbarth, S.; Mendelson, M.; Monnet, D.L.; Pulcini, C.; Kahlmeter, G.; Kluytmans, J.; Carmeli, Y.; et al. Discovery, research, and development of new antibiotics: The WHO priority list of antibiotic-resistant bacteria and tuberculosis. *Lancet Infect. Dis.* **2018**, *18*, 318–327. [[CrossRef](#)]
65. Burkhard, P.; Jagannatha Rao, G.S.; Hohenester, E.; Schnackerz, K.D.; Cook, P.F.; Jansonius, J.N. Three-dimensional structure of O-acetylserine sulfhydrylase from *Salmonella typhimurium*. *J. Mol. Biol.* **1998**, *283*, 121–133. [[CrossRef](#)]
66. Marchetti, M.; Bruno, S.; Campanini, B.; Peracchi, A.; Mai, N.; Mozzarelli, A. ATP binding to human serine racemase is cooperative and modulated by glycine. *FEBS J.* **2013**, *280*, 5853–5863. [[CrossRef](#)] [[PubMed](#)]
67. Karlsson, R.; Katsamba, P.S.; Nordin, H.; Pol, E.; Myszk, D.G. Analyzing a kinetic titration series using affinity biosensors. *Anal. Biochem.* **2006**, *349*, 136–147. [[CrossRef](#)]
68. O’Shannessy, D.J.; Brigham-Burke, M.; Soneson, K.K.; Hensley, P.; Brooks, I. Determination of rate and equilibrium binding constants for macromolecular interactions using surface plasmon resonance: Use of nonlinear least squares analysis methods. *Anal. Biochem.* **1993**, *212*, 457–468. [[CrossRef](#)]
69. Björquist, P.; Boström, S. Determination of the kinetic constants of tissue factor/factor VII/factor VIIA and antithrombin/heparin using surface plasmon resonance. *Thromb. Res.* **1997**, *85*, 225–236. [[CrossRef](#)]
70. Glaser, R.W. Antigen-antibody binding and mass transport by convection and diffusion to a surface: A two-dimensional computer model of binding and dissociation kinetics. *Anal. Biochem.* **1993**, *213*, 152–161. [[CrossRef](#)]
71. Morton, T.A.; Myszk, D.G.; Chaiken, I.M. Interpreting complex binding kinetics from optical biosensors: A comparison of analysis by linearization, the integrated rate equation, and numerical integration. *Anal. Biochem.* **1995**, *227*, 176–185. [[CrossRef](#)] [[PubMed](#)]
72. Gasteiger, E.; Hoogland, C.; Gattiker, A.; Duvaud, S.; Wilkins, M.R.; Appel, R.D.; Bairoch, A. Protein Identification and Analysis Tools on the ExPASy Server. In *The Proteomics Protocols Handbook*; Walker, J.M., Ed.; Humana Press: Totowa, NJ, USA, 2005; pp. 571–607.

- 
73. Annunziato, G.; Pieroni, M.; Benoni, R.; Campanini, B.; Pertinhez, T.A.; Pecchini, C.; Bruno, A.; Magalhães, J.; Bettati, S.; Franko, N.; et al. Cyclopropane-1,2-dicarboxylic acids as new tools for the biophysical investigation of O-acetylserine sulphydrylases by fluorimetric methods and saturation transfer difference (STD) NMR. *J. Enzym. Inhib. Med. Chem.* **2016**, *31*, 78–87. [[CrossRef](#)] [[PubMed](#)]
  74. Manganelli, R.; Voskuil, M.I.; Schoolnik, G.K.; Dubnau, E.; Gomez, M.; Smith, I. Role of the extracytoplasmic-function  $\sigma$  Factor  $\sigma^H$  in Mycobacterium tuberculosis global gene expression. *Mol. Microbiol.* **2002**, *45*, 365–374. [[CrossRef](#)] [[PubMed](#)]